https://doi.org/10.5194/egusphere-2026-787
Preprint. Discussion started: 18 February 2026

Towards Best Practices in UAV Thermal Remote Sensing in Complex Environments

Kathrin Naegeli [1,*], Jennifer Susan Adams [1], Gabriele Bramati [1], Isabelle Gärtner-Roer [1], Julian Gröbner [2], and Nils Rietze [1,3]

[1]Department of Geography, University of Zurich, Winterthurerstrasse 190, 8057 Zurich, Switzerland
[2]Physikalisch-Meteorologisches Observatorium Davos, World Radiation Center (PMOD/WRC), Dorfstrasse 33, 7260 Davos Dorf, Switzerland
[3]Department of Evolutionary Biology and Environmental Studies, University of Zurich, Winterthurerstrasse 190, 8057 Zurich, Switzerland
[*]With the exception of the first author, all remaining authors are listed alphabetically.

Correspondence: Kathrin Naegeli (kathrin.naegeli@geo.uzh.ch)

Abstract. Thermal infrared (TIR) remote sensing using uncrewed aerial vehicles (UAVs) is a promising approach for measuring surface temperatures in complex environments. This study examines the challenges encountered and the lessons learned from UAV TIR surveys of a cryospheric landform in the Swiss Alps. We conducted laboratory experiments and field observations to develop, implement and evaluate the effectiveness of different correction schemes. The results reveal significant dependencies between the internal temperature of the camera and the retrieved surface temperatures, showing a non-linear bias of the UAV TIR camera towards cold, warm, and hot targets. The correction schemes produce divergent outcomes; some amplify extremes, while others reduce the temperature spatial distribution. Validation against data from in situ radiometers and ground surface temperature loggers shows that field calibration provides the most accurate results, whereas drift correction can be misleading in environments with complex topography. By addressing technical and environmental limitations, we provide best practices for UAV TIR surveys and post-processing strategies. Our findings highlight the importance of robust calibration, topographic characterisation and site-specific validation to accurately retrieve surface energy budget-relevant variables in rapidly changing mountainous environments.

1 Introduction

Mountain regions worldwide are experiencing faster warming than the global average with wide-ranging impacts on these ecosystems, and especially the cryosphere (Pepin et al., 2025, 2022). Changes to these systems are manifested by changes in the composition of the Earth's surface materials, such as the transition from ice to rock or grass to shrub. This has a significant impact on the exchange of energy between the surface and the atmosphere, thereby altering the surface energy budget (SEB). Earth system models can quantify the SEB and its dynamics across space and time, and are therefore crucial for determining changes to the SEB under projected warming trends. However, these models rely on an accurate representation of SEB-relevant variables, which are often difficult to acquire in these complex environments, resulting in uncertainties in SEB projections. Land Surface Temperature (LST), a recognised Essential Climate Variable by the Global Climate Observing

https://doi.org/10.5194/egusphere-2026-787
Preprint. Discussion started: 18 February 2026

System, is a fundamental variable in the physics of the surface – atmosphere interface and therefore central to SEB. It is closely linked to the radiative, latent, and sensible heat fluxes and is known to be strongly variable in both space and time (Crago and Qualls, 2014). We can spatially quantify LST from remotely sensed thermal infrared imagery acquired through various emerging technologies like Uncrewed Aerial Vehicles (UAVs), airborne sensors such as HyTES (Hook et al., 2013) or TASI (Pignatti et al., 2011), and upcoming satellite missions such as THRISNA (Thermal infraRed Imaging Satellite for High-resolution Natural resource Assessment, Roujean et al., 2021), SBG (Surface Biology and Geology, Cawse-Nicholson et al., 2021) and LSTM (Land Surface Temperature Monitoring, Koetz et al., 2018).

Traditionally, LST research on cryospheric landforms has relied on either in situ measurements or satellite observations, both of which have limitations in spatial or temporal coverage (Aubry-Wake et al., 2022). However, LST retrieval in complex environments is particularly affected by the small-scale heterogeneity that is impossible to capture with point-scale in situ instruments and coarse-resolution satellite data. Studies have also shown that the up- or down-scaling of LST data in both space and time is challenging, however, and the assimilation of products with an intermediate spatial and/or temporal scale is advantageous (Elfarkh et al., 2023), especially considering the typical ruggedness of mountaineous terrain. UAVs have emerged as an important intermediate platform, capable of bridging the gap between in situ data and satellite remote sensing by providing sub-meter resolution data (Colomina and Molina, 2014; Bhardwaj et al., 2016). The use of UAVs, also carrying thermal sensors substantially increased in recent years (Messmer and Groos, 2024; Bisset et al., 2023; Gök et al., 2023; Kraaijenbrink et al., 2018). Due to the lack of high resolution (sub-meter scale) datasets, synergies between close-range and satellite remote sensing are so far little explored (Kraaijenbrink et al., 2018). Potential mismatches when using these platforms concurrently can mostly be attributed to unknown biases related to scaling effects (Groos et al., 2022) and or survey time differences (Bisset et al., 2023), resulting in divergences of up to several degrees (Kraaijenbrink et al., 2018; Liu et al., 2006). Despite the increased use of UAV Thermal InfraRed (TIR) remote sensing to map LST, many challenges remain in accurately retrieving surface temperatures, particularly in complex environments. These environments are described here as settings with steep topography, strong elevational gradients, and highly heterogeneous (sub-)surface conditions that produce large contrasts in microclimate and surface properties. To take full advantage of technological advances, we must address methodological challenges that complicate LST retrieval in rugged alpine terrain.

Environmental factors strongly influence the accuracy of LST retrieval in complex terrain. Rough surfaces such as rock glaciers or debris-covered glaciers, to name two cryospheric landforms, are particularly affected by shading from steep topography, large elevational gradients, and microclimatic variability that can produce temperature contrasts of several degrees within a single landform (Huo et al., 2021; Brenning et al., 2012). Varying surface materials (e.g. ice cliffs vs. debris, rocky patches vs. vegetation) have different thermal responses that enhance within-flight variability. These effects are further amplified by atmospheric conditions such as wind or sudden cloud cover, which alter both the sensor temperature and the target emission during data acquisition. While satellite sensors with long revisit times often miss such fine-scale variability (Lillesand et al., 2015), UAVs provide the necessary spatial detail to capture it. Their ability to revisit sites and to map parts or entire cryospheric landforms at sub-meter scale makes them particularly valuable for disentangling these environmental drivers of LST variability (Kraaijenbrink et al., 2016). However, assessments of the impact of these contrasting surfaces on the LST re-

https://doi.org/10.5194/egusphere-2026-787
Preprint. Discussion started: 18 February 2026

trieved via UAV or coarser-scale satellite data is lacking in literature. Additionally, without careful correction and calibration, environmental heterogeneity can propagate into consistent errors in subsequent parameter retrieval, such as debris thickness on debris-covered glaciers or snow thermal state to name cryospheric examples (Bisset et al., 2023; Colombo et al., 2023).

Alongside environmental factors, UAV-based TIR measurements face several technical hurdles. Uncooled microbolometer sensors, widely used onboard UAV platforms, are particularly prone to thermal drift as the camera warms or cools during flight. Studies have shown that there is a dependency between the sensor temperature and the retrieved target temperature, with wind and solar irradiance being the most impacting environmental factors affecting this relationship (Gök et al., 2023; Wang et al., 2023; Wigmore and Molotch, 2023; Casas-Mulet et al., 2020; Dugdale et al., 2019; Lin et al., 2018). Therefore, stabilisation of the sensor temperature is key to ensure accurate data acquisition but often required self-made adjustments (Arioli et al., 2024; O'sullivan and Kurylyk, 2022). Various stabilisation strategies, such as allowing pre-flight warm-up time (Kelly et al., 2019) or adding additional flight lines at the beginning of a survey (Bisset et al., 2023), offer only partial solutions, as ambient conditions may continue to change throughout the survey. As complex environments are particularly affected by changing ambient conditions, prior characterisation of the camera in a controlled, laboratory setting could reveal general dependencies that help disentangling artefacts and implementing a drift correction. Additionally, measures like improved mosaicking schemes addressing variable ambient conditions can be of great interest (Malbéteau et al., 2021), but their implementation in complex environments remains difficult. Target-related difficulties compound these acquisition issues. Surface emissivity is often assumed to be uniform, yet it varies substantially across natural landforms, from debris to ice cliffs to snow. If left uncorrected, emissivity variability alone can lead to systematic biases in derived LST (Bisset et al., 2023; Colombo et al., 2023). Calibration strategies such as deploying reference panels or using exposed ice cliffs at 0 °C have been suggested (Gök et al., 2023; Kraaijenbrink et al., 2018), but biases can still fluctuate due to dynamic atmospheric conditions (Maes et al., 2017). These intertwined acquisition and target-related challenges underline the need for systematic laboratory testing and well-designed field campaigns to build more robust correction and calibration frameworks, to leverage the full potential of UAV-based TIR observations over entire landforms situated in complex environments.

Accordingly, the objectives of this study are threefold. Firstly, given the lack of studies focusing on UAV-based thermal infrared applications in complex environments, we present challenges and lessons-learnt arising specifically from these environments, with a focus on cryospheric landforms. We conclude this part presenting a set of recommendations. Secondly, we highlight several post-processing schemes for accurately acquiring absolute surface temperature values from uncooled TIR cameras on board UAV platforms and present a sensitivity analysis. Thirdly, we shed light on the environmental impact on thermal datasets by looking into different topographic metrics within the survey area and at the location of in situ placed sensors. We also discuss their impact on the thematic validations with in situ data. By addressing both environmental and technical obstacles, this work contributes to the improved use of UAV-based TIR data in complex environments, supporting the accurate retrieval of SEB-relevant variables in view for upcoming satellite missions providing TIR data at unprecedented spatial and temporal resolution.

https://doi.org/10.5194/egusphere-2026-787
Preprint. Discussion started: 18 February 2026

2 Study site and data

We conducted UAV TIR surveys over the Murtèl and Marmugnun rock glaciers in the upper Engadine valley in southeastern Switzerland as they have been monitored and instrumented for over 30 years (Gärtner-Roer and Hoelzle, 2021). The area is at the lower permafrost limit and comprises rock glaciers with different activity status, from low-elevation relict rock glaciers in permafrost-free areas to high-elevation, ice-rich active rock glaciers and perennially frozen talus slopes. The survey area is part of the latter and the active rock glacier area comprising both Murtèl and Marmugnun is depicted manually based on RGB and terrain information (Figure 1a). They consist of coarse blocky surfaces with a thickness of about 3-6 m above a 25 m thick ice supersaturated permafrost layer (Saibene et al., 2025). The surveyed area spans an elevation range from 2440 to 2760 m a.s.l. (Figure 1c) and an average slope of 25 ° ± 14 ° (Figure 1e). The rocks consist predominantly of Metagranitoids of all sizes and the vegetation in the lower parts of the survey area is characterised by alpine meadows. We used the UAV RGB imagery to classify the survey area into rock and vegetation (Figure 1d). This is resulting in an object-based emissivity characterisation of the survey area of 0.92 for the pixels classified as rocks (Mineo and Pappalardo, 2021) and 0.96 for the vegetation pixels (Rubio et al., 1997), respectively. The mean air temperature recorded at the station located on Murtèl is -1.66 °C (for the period 1997-2018 (Hoelzle et al., 2022)) and the mean annual precipitation sum at the MeteoSwiss station located at the valley bottom in Sils Maria is 1011 mm, whereas the station on Piz Corvatsch recorded a sum of 1295 mm (for the period 1981-2010).

2.1 UAV-based TIR surveys

The UAV surveys took place on 23 August 2022 and 22 August 2023 in clear-sky conditions around local noon (CEST+2). A fixed-wing eBee X with a Duet T camera (sensefly, https://ageagle.com/drones/ebee-x/) was used. The Duet T camera is a dual mapping system comprising a high-resolution, radiometric thermal infrared camera (FLIR Tau 2) operating in the 8-14 μm range and a S.O.D.A. RGB camera. The flight altitude was with 220 m above ground rather high but needed due to cables obstructing a lower flight level. Each UAV survey lasted for about 20 minutes (23 min in 2022 and 22 min in 2023) and covered a total area of 0.53 km^2. The surveys were planned in way that camera temperature could possibly stabilise before the image acquisition starts. Hence, the UAV take off was at lower elevation in front of the survey area and the flight pattern started in the south-eastern, most elevated corner of the survey area. We flew the UAV in the terrain following flight mode, perpendicular to the solar principal plane to avoid hot spot/glint and large shadowing effects, as well as minimising directionality impacts. To geolocate our images we used Post Processing Kinematic (PPK) with data from the Swiss Positioning Service (swipos). We collected 510 and 501 RGB and thermal images in 2022 and 2023, respectively. This configuration and the use of the Duet T processing work flow and template for the sensefly DuetT camera for pix4d mapper (https://sensefly.zendesk.com/hc/en-us/articles/360013198713-How-to-create-a-Pix4D-project-with-the-senseFly-Duet-T) resulted in RGB and thermal orthomosaics with ∼16 cm Ground Surface Distance (GSD). As a last step, the differently corrected TIR orthomosaics were resampled to 20 cm GSD to ensure optimal comparison between years and datasets.

https://doi.org/10.5194/egusphere-2026-787
Preprint. Discussion started: 18 February 2026

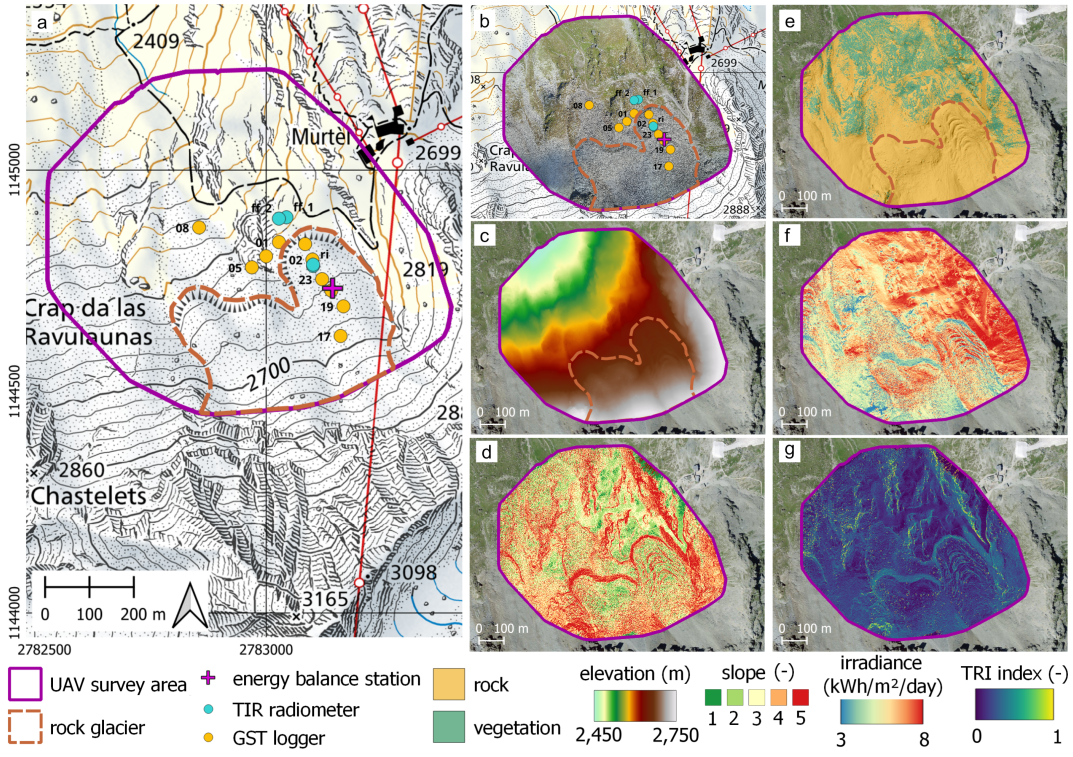

Figure 1. *Study site of rock glaciers Murtèl and Marmugnun in the Engadin valley above Silvaplana. (a) Topographic map (Federal Office of Topography swisstopo) with location of in situ instruments, UAV survey area and rock glacier extent; (b) RGB orthomosaic; (c) digital surface model; (d) slope of UAV survey area in five classes (1: (nearly) flat, 2: gentle, 3: moderate, 4: steep, 5: very steep slope), (e) surface classification, (f) daily sum of solar radiation for DOY 234, and (g) Terrain Ruggedness Index (TRI) after (Riley et al., 1999). (b) to (g) are based on UAV data.*

2.2 Meteorological data

There is a long-term full energy balance station operated by the Swiss Permafrost Monitoring Network (www.permos.ch) located in the centre of Murtèl rock glacier (Figure 1b) providing temporally highly resolved (every 10 minutes) meteorological data. Mean air temperature in the hour spanning the UAV survey was 7.40 ± 0.10°C in 2022 and 15.52 ± 0.39°C in 2023, while the surface temperature at the energy balance station showed greater variability with a mean of 8.29 ± 0.58°C in 2022 and 20.42 ± 1.80°C in 2023. Wind speed was low in both years with 2.55 ± 0.56 m/s and 1.34 ± 0.23 m/s for 2022 and 2023, respectively. Relative humidity was 65 ± 7% and thus considerably higher in 2023 than in 2022 (45 ± 2%). Net shortwave radiation (defined as $SW_{net} = SW_{in} - SW_{out}$) was slightly higher and less stable in 2023 (663 ± 159 Wm^{-2}) than in 2022 (602 ± 23 Wm^{-2}). Net longwave radiation (defined as $LW_{net} = LW_{in} - LW_{out}$) was very similar in both years with −120 ± 2 Wm^{-2} and −118 ± 3 Wm^{-2} for 2022 and 2023, respectively. Details about the meteorological conditions two days prior and past the survey day, as well as ±30 minutes from the start of the UAV survey can be found in the Supplementary Figures A1 and A2.

https://doi.org/10.5194/egusphere-2026-787
Preprint. Discussion started: 18 February 2026

2.3 Auxiliary data

During the survey in 2022, four thermal infrared radiometers (Apogee, SI-121-SS) were installed (Figure 1b): while two were placed in vegetated locations in front of Murtèl, one was placed on a ridge and one in a furrow in the lower third of the rock glacier. The TIR radiometers are operating in the 8-14 μm range with a 18° half angle FOV. Their stated accuracy is 0.2 °C from −30 to 65°C, when the Δ temperature between target and sensor is <20°C, and 0.6 °C when Δ temperature is >20 °C. All radiometers provided us with temporally highly resolved (10 minutes) radiometric skin temperature information encompassing different footprint sizes (1.6 – 18.8 m^2) depending on installation height and angle.

Additionally, we had access to Ground Surface Temperature (GST) data at 10 different locations (nine UTL loggers v2 and v3, and one GEO PRECISION M-Log5W, Figure 1b), four in the forefield and on the relict part of the rock glacier, and six on the rock glacier itself, that provide contact skin temperature data of the top part of the active layer at 60-90 minutes intervals. The stated accuracy of both logger models is 0.1 °C.

During the survey in 2023, only one thermal infrared radiometer was still installed on the ridge of Murtèl. Simliarly, GST loggers were available but some couldn't be accessed since due to large rock fall activities. Thus, for four GST loggers we do only have data from just the days before the UAV survey, but in similar meteorological conditions (Supplementary Figure A2), and one GST logger was buried ('GST-017').

For validation purposes, we built 0.6 x 0.6 m Thermal Calibration Plates (TCPs) following suggestions by Kelly et al. (2019). These side lengths are about 3.75 times larger than the GST of the TIR mosaics. We used a 1 mm thick aluminium sheet underlaid by a 20 mm thick expanded polystyrene plate for isolation and a 4 mm thick wooden plate for stabilisation purpose. A surface contact PT100 (OMEGA SA1-RTD-4W) was attached to the underside of the aluminium sheet, which was painted with black paint with known emissivity (ε = 0.963, HERP-LT-MWIR-BK-11 from LabIR). Temperature readings were recorded using a blueDAN Pt100_4.0 logger every 30 seconds.

2.4 Topographic characteristics at validation locations

To assess possible impacts of topographic characteristics on the absolute deviation between in situ observations and TIR mosaics, five topographic metrics, elevation, slope, aspect, small scale terrain roughness and the irradiance received by the instrument location prior to the UAV survey were assessed. Figure A4 presents these characteristics per individual TIR radiometer and GST location.

The in situ sensors were spread out over an elevational gradient (>120 m) spanning from 2572 to 2693 m a.s.l. Similarly, the average slope characteristics varied from being flat (1.4° at 'GST-04') to very steep (40.4° at 'GST-03'), with an average of 19.2° ± 11°. Moreover, the variability of slopes (standard deviation) extracted within the footprint of each location varied greatly from ± 1.2° to ± 19.3° (mean 8.3° ± 6.2°), highlighting the very heterogeneous surface characteristics of some in situ instrument locations. This terrain heterogeneity was also well depicted in the Terrain Ruggeddness Index (TRI) (Riley et al., 1999) that showed a range of values from 0.01 to 0.42 (mean 0.17 ± 0.12) depending on the in situ location. The global total irradiance (see section 3) received at each in situ location varied considerably from 4494 $Whm^{-2}day^{-1}$ at minimum (TIR

https://doi.org/10.5194/egusphere-2026-787
Preprint. Discussion started: 18 February 2026

radiometer 'fu') to 7470 $Whm^{-2}day^{-1}$ at maximum ('GST-04'), with an average of 6494 ± 911 $Whm^{-2}day^{-1}$ over all in situ locations. Also, the variability of global total irradiance (standard deviation) received within the footprint of each location showed great difference from almost none with 109 $Whm^{-2}day^{-1}$ (TIR radiometer 'ff2') to massive with 1515 $Whm^{-2}day^{-1}$ ('GST-21').

3 Methdology

Within this study, we define ***complex environments*** as follows:

- **complex topography** (high altitude sites, large topographical gradients within and surrounding the surveyed landform, remote and hardly accessible) and/or
- **high elevation and/or high elevational gradient** (large gradient in atmospheric conditions within the survey area) and/or
- **large variance of slope and aspects** (high surface ruggedness) and/or
- **little surface contrast** (uniform surface morphologies/type) and/or
- **high spatial heterogeneity** (small-scale characteristics within survey area) and/or
- **complex sub-surface - surface - atmosphere energy exchange** (varying sub-surface materials, heterogenous turbulent and ground heat fluxes) and/or
- **harsh environmental conditions** (very cold, winds, great Δ-temperature between sensor and target)

To shed light on different challenging impacts on the processing of UAV TIR data in complex environments, we tested different corrections, from laboratory to field-based, taking variations of the ambient meteorological conditions during the survey into account as well as solely the internal camera temperature. Moreover, the RGB orthomosaic and DSM were used to compute an object-based surface classification (Figure 1e), which itself is the basis for the spatially distributed emissivity characterisation based on literature values. The computed slope, aspect and DSM served as inputs to compute the irradiance distribution, the total amount of energy received per square meter over the course of one day (doy = 234 in 2023) calculated using the R.sun.insoltime tool in QGIS (https://grass.osgeo.org/r.sun.html) for the greater survey area. Each correction scheme is characterised by specific processing steps, which we outline hereafter in detail.

To account for the local atmospheric conditions during the surveys (T_{corr_ATMO}, see Figure 4), we converted the raw binary FLIR images to temperature utilising the R raw2temp function (Tattersall, 2021). The function applies standard radiometric calibration processing equations of thermal infrared images, taking into account the FLIR camera calibration coefficients and local environmental conditions including air temperature, relative humidity and distance to object. Most UAV processing softwares apply these formulae using standard values of environmental variables, thus we updated the conversion using the

https://doi.org/10.5194/egusphere-2026-787
Preprint. Discussion started: 18 February 2026

aforementioned variables monitored by the meteorological station during the survey and the UAV-surface distance used in the survey flight planning (220 m).

Finally, all TIR orthomosaics are emissivity corrected using the emissivity characterisation and the sky temperature T_{bg} following Maes and Steppe (2012):

$$T_{bg} = \sqrt[4]{\frac{LW_{in}}{\sigma}} \tag{1}$$

and

$$T_{corr\_EMI} = \sqrt[4]{\frac{T_{meas}^4 - (1-\varepsilon) \cdot T_{bg}^4}{\varepsilon}} \tag{2}$$

to obtain emissivity corrected radiometric skin temperature T_{corr_EMI}. With LW_{in} denoting the incoming longwave radiation, σ the Stefan-Boltzmann constant, ε the emissivity, and T_{meas} the radiant temperature obtained from the UAV TIR camera. An overview of our full methodological workflow is shown in Figure 4.

3.1 Camera - Target dependency correction based on laboratory experiment

In order to investigate the effect of camera – target temperature dependency, we performed laboratory experiments with our DuetT camera at the Physical Meteorological Observatory in Davos (PMOD) World Radiation Centre (WRC) blackbody calibration facilities. The camera was facing into a black body cavity, BB2007, that consists of a custom-made cylindrical cavity with an inclined bottom and an effective emissivity of 0.99993±0.00033 (Gröbner, 2008). Images were acquired every 30 seconds and the experiments lasted several hours to allow the black body to stabilise at varying temperatures likely to be encountered at the rocky surface of a rock glacier in summer (0°, 15°, 20°, 30°). The radiation temperature at the output aperture of the blackbody is traceable to the SI with a standard uncertainty of 0.05 K. The camera was exposed to simulated wind to (i) not overheat and (ii) have varying camera temperatures alongside stable black body temperatures. Other ambient conditions were kept constant in order to clearly identify the dependence between camera and image temperature.

For further analyses, we only used the images that were taken in periods when the black body was stable, i.e. standard deviation smaller than 0.15°C. This left us with 149 individual images from which we extracted a central area of 320 x 320 pixels, which we were confident represented the centre of the blackbody and thus limitedly impacted by vignetting effects. From this central area, we randomly sampled 500 pixels, assigned 80% of them to train a correction model and 20% to validate it. Additionally, the camera temperature for each of these images and the relating black body temperature were extracted from the metadata. Based on these observations, a second order polynomial multivariate regression model was fit to the data, given inputs T_{raw} and T_{camera}:

$$T_{corr\_LAB} = 0.0 + 1.335T_{raw} - 0.327T_{camera} + 0.004T_{raw}^2 - 0.020T_{raw} \cdot T_{camera} + 0.010 \tag{3}$$

https://doi.org/10.5194/egusphere-2026-787
Preprint. Discussion started: 18 February 2026

Figure 2a shows the results of the final model on the validation dataset. The model is able to reduce RMSE from 1.98°C to 1.086°C. Higher order polynominal models were tested and resulted in better RMSE, but were omitted as the risk of overfitting temperatures above and below the blackbody temperatures is too high. Figure 2b shows the ratio between image temperature and blackbody temperature with regards to camera temperature, and associated histogram of values (Figure 2c). The correction model improves reproduction of the blackbody temperature significantly (when ratio equals 1), particularly for lower camera temperatures.

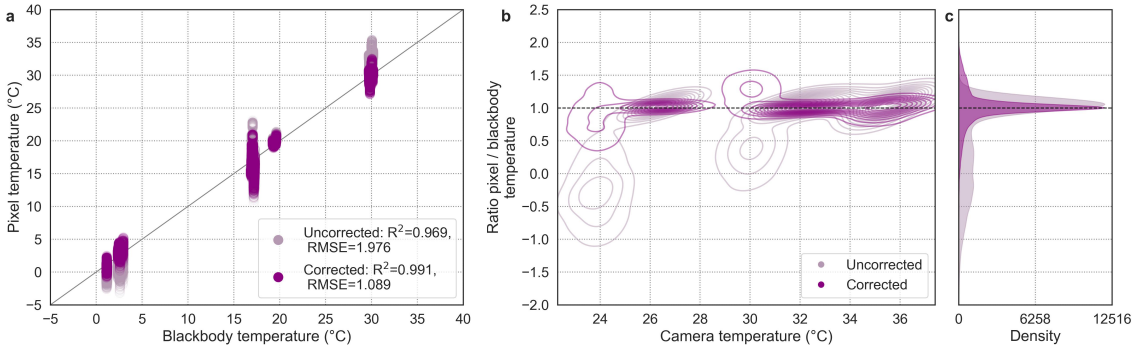

Figure 2. *Blackbody reference temperature and associated measured pixel temperature for uncorrected and corrected data using lab correction model (a), and ratio of pixel temperature to blackbody temperature with respect to camera temperature shown as a Guassian kernel density plot (b) and distribution of ratio values (c) for uncorrected and corrected data.*

3.2 Camera temperature based drift correction

To correct for the impact of changing camera temperature on the measured pixel temperature, we applied an image-based method adapted from Mesas-Carrascosa et al. (2018) and first used on DuetT thermal imagery in the Arctic tundra in Rietze et al. (2024). This method shifts images by an empirically derived correction temperature (T_{corr}) in the camera's adjustment phase, i.e. during the time it takes for T_{camera} to stabilise. Consequently, images taken during camera stability (when T_{camera} <$T_{camera,min}$ ± 0.1°C) were not corrected. First, a quadratic function to the relationship between T_{corr} and T_{camera} is fitted to retrieve the fitted T_{corr} for any given T_{camera}:

$$T_{corr} = a \cdot T_{camera}^2 + b \cdot T_{camera} + c \quad (4)$$

where T_{corr} is defined as the deviation of the mean temperature of an individual image ($\overline{T}$) over the period of camera instability from $\overline{T}$ during camera stability. Second, T_{corr} is subtracted from each pixel (T_{raw}) in the entire image resulting in drift-corrected T_{corr_DRIFT}:

$$T_{corr\_DRIFT} = T_{raw} - T_{corr} \quad (5)$$

https://doi.org/10.5194/egusphere-2026-787
Preprint. Discussion started: 18 February 2026

3.3 Field thermal calibration using TCPs

In 2023, two TCPs were placed on the rock glacier, and one TCP was placed close to the take off and landing point of the UAV to obtain hand-held imagery before and after the survey. The latter TCP was covered with a white blanket and kept in the shade to obtain warm values (pre-survey). Consequently, the same TCP was left exposed to the solar radiation and thus quickly heated up providing us with a hot (pre-survey) and very hot (post-survey) temperature target. A set of hand-held images (n=9) were taken over the TCP in all three temperature conditions. An average image temperature was extracted form all individual 27 images around the image centre (320x320 pixels). These average image temperatures were corrected for the emissivity of the black paint (see Auxiliary data) that we used to coat the TCPs by a simple emissivity correction not taking into account the reflected radiation from the background. For each target temperature the calculated mean of nine average image temperatures were compared to the measured TCP temperature. The resulting linear model (Figure 4) was used to correct the 2023 UAV-based TIR images:

$$T_{corr\_FIELD} = 0.85 \cdot T_{raw} + 6.35 \tag{6}$$

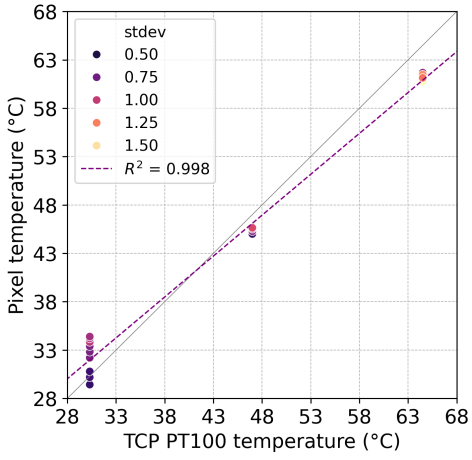

Figure 3. *Comparison of pre- and post-flight temperature from the PT100 attached to the TCP and the extracted mean pixel temperature from the hand-held UAV TIR camera imagery (n=27) in 2023. Brighter datapoints exhibit larger pixel temperature variability than darker ones.*

3.4 Auxiliary data pre-processing

3.4.1 TIR radiometer correction

Correction for surface emissivity is required for accurate temperature measurements also with TIR radiometers. Radiation received by a sensor is thus comprised of the radiation emitted by the surface and the radiation reflected from the background.

https://doi.org/10.5194/egusphere-2026-787
Preprint. Discussion started: 18 February 2026

Temperatures measured from the Apogee radiometer were corrected according to equation (1) and (2) introduced above. Emissivity information for the TIR radiometer location was taken from the object-based emissivity classification (see section 2) and background temperature was derived based on data from the AWS (see section 2.3).

Calibration of the SI-121-SS is traceable to NIST, however sensor temperature of this uncooled radiometer is known to impact measurement of target temperature and may become biased after their initial calibration (Aragon et al., 2020). Therefore, sensor-target temperature dependency of the TIR radiometers was characterised in the lab following a similar protocol as outlined for the UAV camera and with the same blackbody cavity. A dedicated copper casing for the TIR radiometer was developed to efficiently dissipate heat from the heating plate of the blackbody to alter the sensor temperature. Both the blackbody reference target temperature and the TIR radiometer sensor temperature were set to measure between 0 and 40°C in steps of 10°C. Delta temperature between blackbody and sensor was never more than 20°C, thus following measurements were made of *blackbody* and sensor (in brackets): *40* (20, 30, 40), *30* (40, 30, 20, 10), *20* (0, 10, 20, 30, 40), *10* (30, 20, 10, 0) and *0* (0, 10, 20). Each blackbody/sensor configuration lasted 40 minutes (approx. 20 min to stabilise, and 20 min for stable measurements), with both the TIR radiometer and the blackbody measuring at 30 seconds frequency. TIR radiometer measurements were integrated over 10 seconds. Finally, a model was developed to correct the measured target and sensor temperature to the blackbody using a 2nd order multivariate polynomial linear regression (Adams et al., 2025).

For the final validation of in situ TIR radiometer data with the differently corrected UAV TIR mosaics, the correction including local emissivity information, the background temperature estimated from incoming longwave radiation measured at the energy balance station and the laboratory correction for the sensor-target dependency was applied.

3.4.2 Pixel extraction

As the TIR radiometers recorded an average temperature of an ellipsoidal footprint, a radiometer specific area (see section 2.3) was extracted from each mosaic for the validation. For the extraction of the pixels around the GST locations, the spot-size-effect (https://www.flir.eu/) of the thermal camera and the survey characteristics were taken into account. For our surveys, the spot-size is calculated to be 0.34 m (1x1 pixel) and approximately 1 m for 3x3 pixels. Consequently, a circular buffer of 1 m diameter was laid around each GST location to extract the mean and standard deviation for both the temperatures of the different TIR mosaics and the varying topographic characteristics.

3.5 Validation, sensitivity analysis and topographic impact assessment

The outlined correction schemes were implemented at the image level. The final corrected mosaics were validated by calculating the absolute temperature difference between each individual mosaic and the in situ data. To assess the sensitivity of the raw TIR mosaic to individual correction schemes, the temperature distribution and deviations per and in between mosaics were investigated. To shed light on the impact of topographic characteristics, five different metrics (elevation, slope, aspect, TRI and irradiance, Figure 1) were extracted per in situ sensor location (see Figure A4), and their mean and standard deviations correlated with the mean absolute temperature difference obtained from the validation (see Figure A5). A summary of our methodology workflow is presented in Figure 4.

https://doi.org/10.5194/egusphere-2026-787
Preprint. Discussion started: 18 February 2026

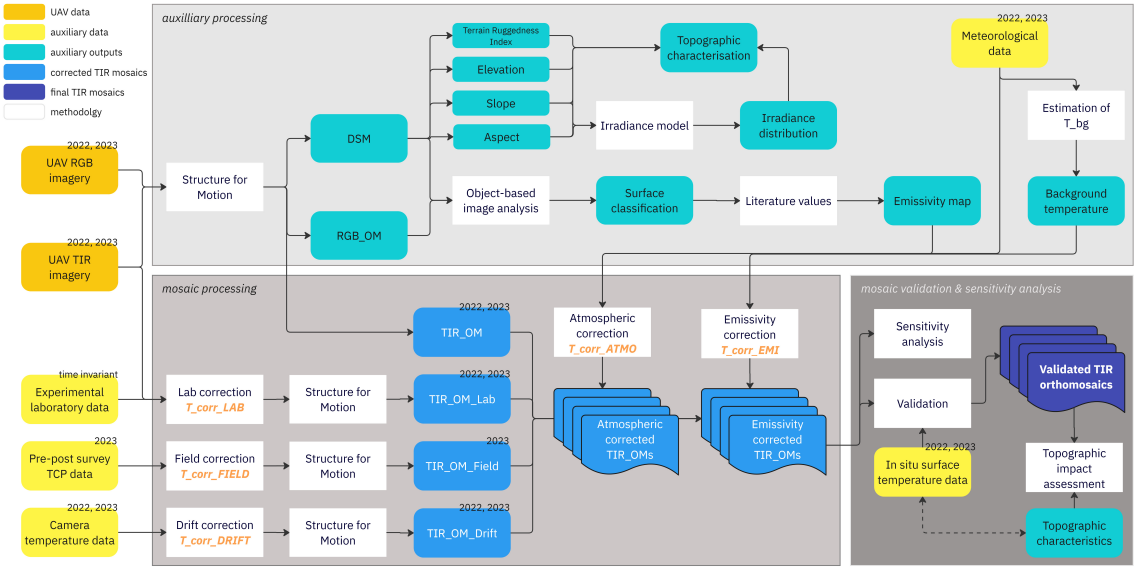

Figure 4. *Methodology flowchart showing the auxiliary processing based on the UAV data (top), the processing from individual images to mosaics (bottom left), and the validation and sensitivity analysis of the mosaics, as well as the topographic impact assessment (bottom right).*

4 Results

4.1 Camera - pixel temperature dependency

The laboratory experiments revealed that camera temperature fluctuations drive instability in recorded pixel temperatures, independent of blackbody temperature setpoints (Figure 5 a-e for individual experiments and f in summary). For clarity of comparison, all temperature time series were detrended by subtracting their respective mean values, thereby removing absolute offsets and emphasizing relative temperature fluctuations between the camera, pixels, and blackbody. The correlation between camera and pixel temperature was positive and stronger for warmer blackbody temperature, and negative and weaker for blackbody temperature close to zero. This reflects the camera specifications stating a decreasing accuracy with increasing Δ temperature between target (i.e. blackbody) and sensor (i.e. camera).

The absolute comparison of blackbody versus pixel temperatures indicated the underestimation of cold and the overestimation of warm blackbody temperatures, respectively (Figure 6). Experiments that display a wider range of pixel temperatures to capture the stable blackbody temperature, are characterised by greater fluctuations in camera temperature (Figure 5f) as well as hotter camera temperatures (Figure 6), highlighting again the strong dependency between camera and pixel temperature.

https://doi.org/10.5194/egusphere-2026-787
Preprint. Discussion started: 18 February 2026

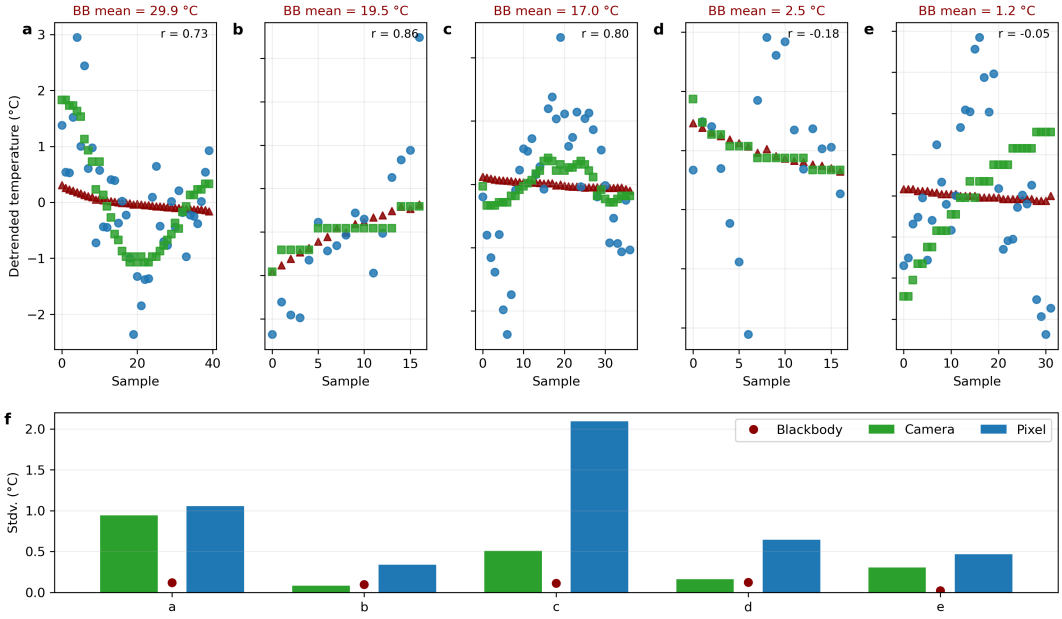

Figure 5. *Detrended time series of pixel (blue), camera (green), and blackbody reference temperature (darkred) for five experiments with different blackbody setpoints (a–e). Correlation coefficients (r) between camera and pixels temperatures are shown in the upper right of each panel. Panel f summarizes the variability (standard deviation) of camera, pixel, and blackbody temperatures for all experiments.*

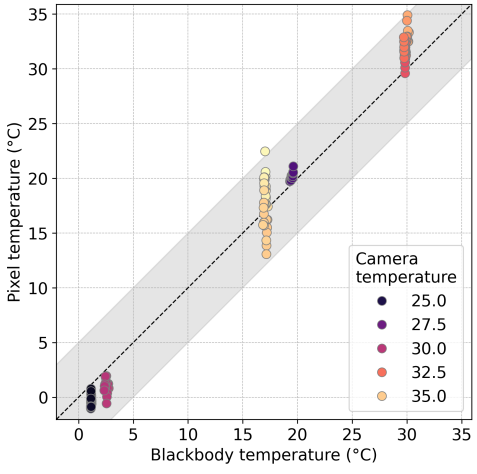

Figure 6. *Relationship between blackbody and pixel temperature for all experiments. Each point represents one image (n=27), colored by its camera temperature. The dashed line indicates the 1:1 relation, with the shaded area marking the accuracy range of ±5°C provided by FLIR for the camera model Tau 2.*

https://doi.org/10.5194/egusphere-2026-787
Preprint. Discussion started: 18 February 2026

4.2 Camera temperature based drift correction

The internal temperature of the camera (T_{camera}) cooled down in the first minutes of both surveys impacting the surface temperature observations (Figure 7 a and b). The R^2 of the fitted models was 0.79 and 0.86 for 2022 and 2023, respectively, indicating a good fit (Figure 7 c and d). The temperature of the raw images (T_{raw}) at the point of highest camera instability had to be corrected by up to approximately 10 and 15°C in 2022 and 2023, respectively.

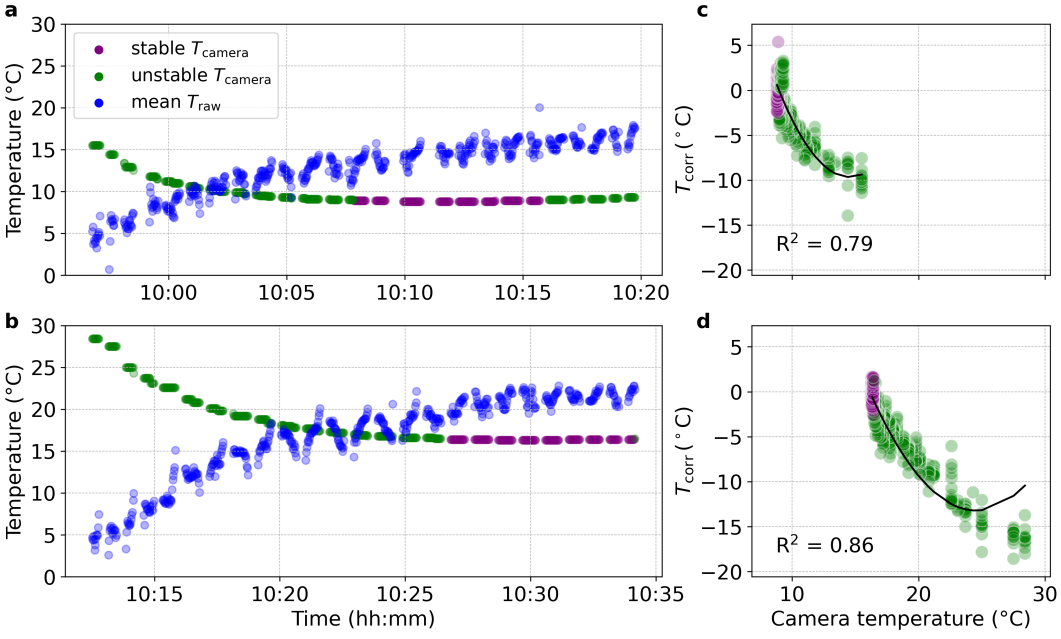

Figure 7. *Camera – pixel temperature dependency during both survey in 2022 (a) and 2023 (b). Time shown in a and b is GPS time. Relationship between camera temperature and correction temperature (T_{corr}) in 2022 (c) and 2023 (d).*

4.3 Field thermal calibration

The warm target was overestimated by 2.06 °C, while the hot and very hot targets were underestimated by 1.65 °C and 3.24 °C, respectively (Figure 3). The greatest variability was observed for the very hot target temperatures with an average standard deviation of 1.15 °C, and considerably lower average standard deviations of 0.77 and 0.62 for the warm and hot targets, respectively. Overall, this pre- and post-survey thermal field calibration revealed an accuracy of the mean image pixel temperatures of -0.95 ± 0.85 °C, which is far below the stated accuracy for the camera model of ±5°C, and even including outliers of up to +4.09 ± 0.91 °C and -3.74 ± 1.60°C.

https://doi.org/10.5194/egusphere-2026-787
Preprint. Discussion started: 18 February 2026

4.4 Sensitivity analysis for applied correction schemes

The corrections outlined above have varying impact on the mean pixel temperature of the orthomosaics but also the spatial distribution of pixel temperatures within the entire surveyed area (Figure 8). The drift correction has the greatest impact on the observed temperature (Figure 9 and Table A1). While it warms the mosaic overall by 20% (+2.72 °C) and 45% (+7.32 °C) on average for 2022 and 2023, respectively, the range of temperature values was attenuated, i.e. a reduction in temperature gradient across the mosaic was observed (Table A1). Particularly, the south-eastern corner of the mosaic, which was overflown first and affected by changes in camera temperature the most, is impacted by this correction scheme most (Figure 8).

The correction based on laboratory analysis shows only small deviation from the raw mosaic, with slight warming of 3.5% on average in 2022 and negligible cooling of -0.1% on average in 2023, and a slight attenuation of minima and maxima, as well as outlier temperatures. In contrast to the drift correction, which also shows substantial impact, the field thermal calibration using TCPs implemented on the 2023 data cools the mosaic by 27% (-4.04 °C) on average and amplifies the range of observed values by over 10 °C (Figure 9).

4.5 Validation with in situ data

The availability of TIR radiometer and GST data allows for an absolute validation of all TIR OMs keeping in mind that the instruments (UAV TIR camera, TIR radiometers ('ff1', 'ff2', 'ri', 'fu') and GST loggers ('01' to '23') are based on different measurement principles (i.e. contact skin versus radiometric skin temperature measurements), affecting the direct comparison. Figure 10 shows the greatest deviation between TIR OM and in situ data for the drift corrected mosaics in both years with absolute differences up to ∼20 °C. The laboratory correction scheme corrected mosaic showed similar validation performance as the raw TIR OMs for both years, with generally less deviations compared to the drift corrected ones, but still differences up to about 15 °C. The smallest absolute differences are observed for the field corrected TIR OM in 2023, with most absolute deviations around 1 to 5 °C.

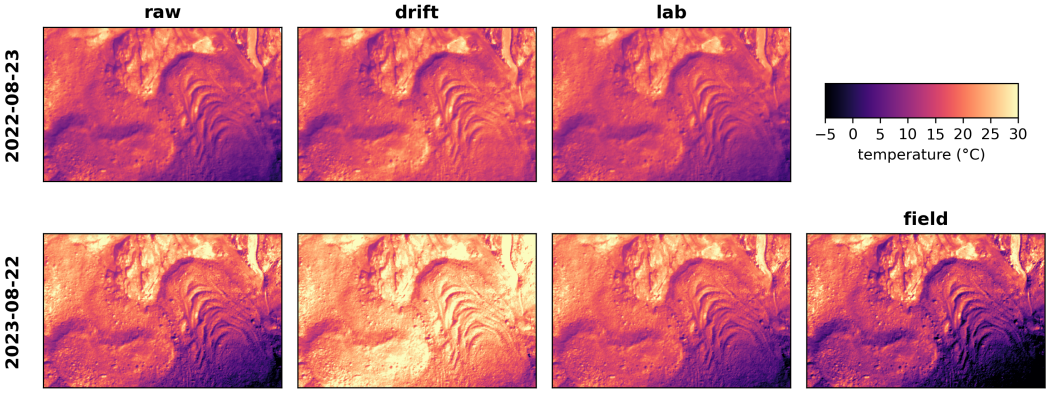

Figure 8. *Thermal orthomosaics from both survey years (top: 2022, bottom: 2023) and varying correction schemes (raw, drift, lab and field).*

https://doi.org/10.5194/egusphere-2026-787
Preprint. Discussion started: 18 February 2026

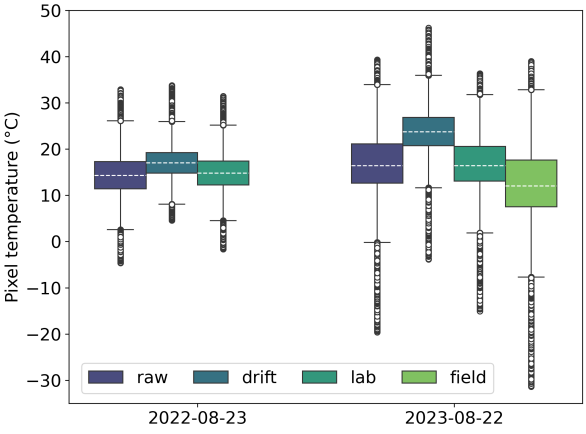

Figure 9. *Sensitivity of thermal UAV mosaics to different correction schemes. Boxplots illustrate pixel temperature distributions (°C) for raw, drift-, lab-, and field-corrected mosaics on the two survey dates, highlighting the influence of correction choice on the resulting thermal patterns. White dashed line indicates mean value of each orthomosaic.*

Focusing on the individual in situ measurement locations, clearly 'GST-03', 'GST-04', 'GST-05' and 'GST-08' show greatest deviations, all above 11°C and up to over 20°C. In contrast, 'GST-01' and the two radiometers 'fu' and 'ff2' show the most similar temperatures compared to all TIR OMs. The remaining GST locations ('GST-02', 'GST-17' to 'GST-23') and the two radiometers ('ff1', 'ri') show medium deviations in the range of about -4 to 8 °C, except for higher differences if compared to temperature recorded in the drift correct TIR OM.

Recalling the topographic characteristics per in situ sensor location (see section 2.3), most locations with very steep slopes (slope 40°), high surface roughness (TRI ∼>0.2) and/or high amounts of received irradiance (>7000 $Whm^{-2}day^{-1}$) are performing worst. In contrast, most locations with a performance accuracy <5°C are topographically inconspicuous or show only one elevated characteristic.

In light of the stated accuracy range of ± 5 °C of the UAV TIR camera, two radiometers show deviations within this range, one is very close to this range, and one is off by over 3.5 °C (column 'ave' in Figure 10). Generally, the deviations with the GST sensors are greater and only three are within the accuracy range of the UAV TIR camera.

Overall the TIR OMs corrected with the lab or field correction scheme performed similar to the raw OMs in both years (row 'ave' in Figure 10). The drift corrected TIR OMs show far greater deviations with over 8 and 12 °C in 2022 and 2023, respectively. The best validation performance, with an absolute difference of ∼6.5 °C on average (∼4 °C if the three strongest outliers ('GST-08', 'GST-03' and 'GST-04') are omitted), was found for the TIR OM corrected with the field thermal data in 2023.

https://doi.org/10.5194/egusphere-2026-787
Preprint. Discussion started: 18 February 2026

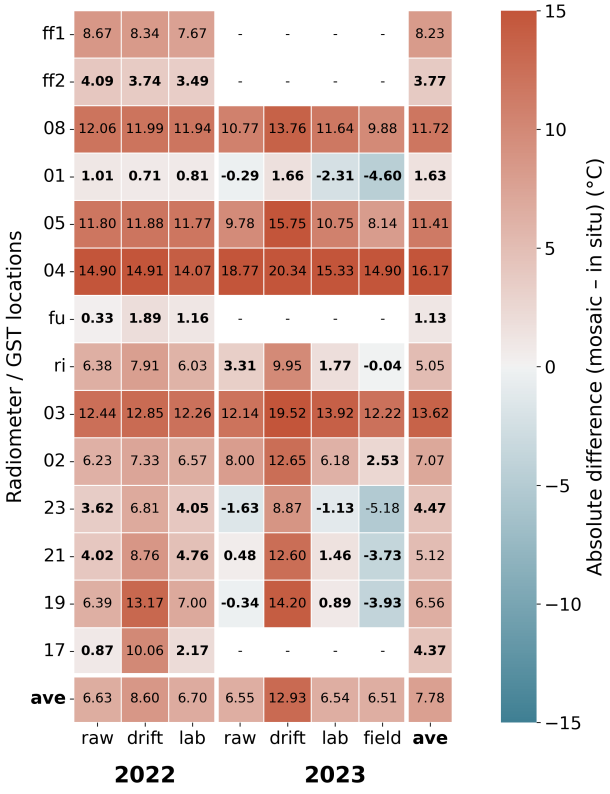

Figure 10. *Heatmap of the absolute validation of TIR OMs with in situ data for 2022 (left three columns) and 2023 (right four columns), including row and column averages (right and bottom most). Rows are labelled according to the GST/radiometer ID (Figure 1a). Positive values (red) indicate warmer, negative values (blue) indicate cooler TIR OM surface temperatures compared to the in situ data. Bold values mark deviations within the accuracy range of the UAV TIR camera.*

5 Discussion

We conducted various laboratory and field experiments with our UAV TIR camera to characterise its behaviour in response to changing ambient conditions, the dependency between the internal camera temperature and the pixel temperature, and its ability to accurately observe temperatures ranging from cold to very hot. These experiments revealed various challenges and enabled us to develop correction schemes. Based on our lab and field experiments, we demonstrate the UAV TIR camera's non-linear accuracy behaviour towards cold (underestimation), warm (overestimation) and hot (underestimation) target temperatures. Furthermore, the experiments revealed a strong relationship between camera and pixel temperatures, showing that greater variations in the former result in greater variations in the latter. They also demonstrated that this impact increases if the temperature difference between the target and the camera increases. Of the applied correction schemes, the drift correction warms the OM on average, while the field correction scheme cools it, and the lab correction scheme has a negligible impact on the average mean OM temperature. Validation using in situ observations revealed that the field correction scheme performed

https://doi.org/10.5194/egusphere-2026-787
Preprint. Discussion started: 18 February 2026

best, with the smallest absolute deviations. Our findings emphasise the importance of careful data acquisition planning, camera characterisation, and highlight the need for and potential of field calibration.

5.1 Prior to data acquisition

Although the lab-based correction scheme had the smallest impact on mean absolute surface temperature it is crucial to gather as much knowledge on temperature dependent camera characteristics in a controlled laboratory setting to ensure minimal surface temperature orthomosaic falsification due to camera internal behaviour. Similarly, experiments should be performed to characterise in situ instruments and their behaviour towards changes in ambient conditions, internal temperature variations and Δ temperature between sensor and target.

Besides these lab-based preparatory analysis, a thorough analysis of the survey area in terms of topographic characteristics is inevitable in complex environments. Small-scale heterogeneity can be demonstrated by calculating metrics such as the TRI or the spatial distribution of pixel-based received irradiance prior to the planned survey. Classic topographical parameters such as slope, aspect and elevational gradient further help to best characterise the study site and understand surface temperature patterns. Such a detailed investigation of the field site enables the most effective planning of thematic validation, ensuring that the spatial heterogeneity of emissivity, topography, and the resulting surface temperature in the survey area are captured optimally.

Additionally, the flight planning in complex environments is absolutely crucial. The acquisition pattern should be designed based on the characterisation of the UAV TIR camera and the field site. Terrain following flight mode is highly beneficial for sites with large elevational gradients. In order to accurately retrieve surface temperatures, it is necessary to minimise the effects of directionality by taking the flight geometry into account in relation to the position of the sun. Although a survey conducted around local noon is ideal, local topographic characteristics (e.g. shading) may necessitate an earlier or later acquisition time.

5.2 During data acquisition

The field-based correction scheme resulted in best validation results highlighting the value of in-field calibration efforts, also shown by other studies (e.g. Wan et al., 2024). The deployed TCPs in the survey area were not useful due to the strong adjacency effects in the data, which resulted from their relatively small size compared to the GSD obtained from the UAV, as well as the spot-size effect of the camera itself. However, in the case of our study area and flight constellation (i.e. flight height of 220 m above ground) a suitable TCP within the survey area would need to have a side lengths of at least 3 m, ideally even more, which is not feasible to bring and deploy in this high altitude, complex terrain.

In contrast, the TCP used to calibrate the camera with handheld pre- and post-survey imagery revealed to be of great help. However, the absolute and range of temperature values covered by this TCP were far from ideal as they did neither mimic the absolute nor the distribution of temperature in the survey areas a suggested by Kelly et al. (2019). This likely explains parts of the still multiple degrees of absolute temperature difference with most validation sites.

Furthermore, the positioning of certain GST instruments hampers validation performance as they are heavily shaded by a large boulder, resulting in different temperature readings to those observed by the UAV TIR camera. Similarly, locations

https://doi.org/10.5194/egusphere-2026-787
Preprint. Discussion started: 18 February 2026

that receive great amounts of irradiance prior to the UAV flight heat up more, resulting in higher radiometric temperatures observed by a UAV TIR camera. In contrast, these locations exhibit a lagged temperature cycle in the measured skin temperature culminating with maximum daily temperatures around mid- to late afternoon (Figure A3) limiting direct validation.

While the existing full energy balance station records data every ten minutes, we still noted changing ambient conditions in our field journal. In 2023, the occurrence of few clouds in the vicinity of our survey area, was also visible in the shortwave incoming radiation data. This helped to understand the slight dip in the warming of the GST sensors (see 'GST-01' or 'GST-03' in Figure A3). This might also explain parts of the contrasting general temperature behaviour, i.e. underestimation of a few, most elevated GST locations, compared to 2022.

5.3 Post data acquisition

We clearly detected cooling of the camera temperature in the beginning of both of our surveys. However, the drift correction applied does not seem to be the ideal correction scheme for surveys conducted in complex environments. While this correction was developed for flat tundra sites, our field site was affected by varying degrees of shading due to the surrounding topography, which most likely induced surface temperature gradients across the survey area and affects local thermal inertia. This is also supported by the calculated spatial pattern of the total global irradiance received before the survey. It is nearly impossible to disentangle the effects of these multiple factors on surface temperatures, as well as on the UAV TIR camera and the in situ instruments. However, our validation results clearly showed the worst performance of the drift-corrected OMs, indicating its limited applicability in complex environments. Nevertheless, we strongly recommend extracting the internal camera temperature throughout the survey and considering correction schemes to account for variability or omitting parts of the surveyed area.

Generally, validation is hampered by the increasing complexity of the area studied. For example, areas with greater slopes are likely affected by directional effects impacting the accurate retrieval of LST from UAV data, or large small-scale heterogeneity of surface characteristics within the UAV footprint (i.e. GSD- and spot-size effect-dependent) limit validation accuracy, just to mention two examples. We calculated Pearson correlation coefficients between in situ and UAV TIR absolute temperature differences and means and standard deviations of topographic factors (Figure A5). While analysing mean values provides insight into local topographic characteristics and their potential impact on validation performance, analysing standard deviations reveals the potential impact of local heterogeneity on validation performance. The impact of these factors is expected to be particularly severe in complex environments. A moderate positive correlation was found for mean irradiance, indicating its strong importance for accurately retrieving surface temperature information (Figure A5a). Interestingly, we found mostly negative correlations between standard deviations and absolute UAV - in situ temperature differences, indicating that increasing heterogeneity leads to decreasing mismatch between UAV and in situ (Figure A5b). This suggests that in more heterogeneous terrain, UAV TIR OMs tends to average over the spatial heterogeneity, making the UAV observation more representative. However, it should be noted that none of the correlations were significant, which may be due to the limited number of validation locations. A more detailed analysis with a greater sample size, or a comparative study of a complex and non-complex environment, would be of great interest and likely reveal more robust results.

https://doi.org/10.5194/egusphere-2026-787
Preprint. Discussion started: 18 February 2026

5.4 Uncertainties and limitations

The object-based emissivity representation ignores mixed-pixel effects, and single literature-based values neglect the local characteristics. While the mixed-pixel effect in the case of a UAV survey and a respective GSD of 20 cm in our survey area is minimal, the literature-based emissivity values are rough assumptions and hence may impact surface temperature retrieval considerably. We tested this impact by increasing and decreasing the fixed emissivity values by 0.01, resulting in an average (over all corrections) decrease and increase in mean OM temperature of 0.2 °C, respectively.

The assumption of spatio-temporally constant local environmental conditions during the survey impacts the radiometric calibration and atmospheric correction. However, considering the survey duration of roughly 20 minutes and the stable weather situation, this effect is likely negligible. Meteorological data with higher temporal resolution from multiple locations within the survey area would be needed to investigate and quantify this uncertainty.

Adjacency effects are critical when spatial heterogeneity is large (Aubrecht et al., 2016), as indicated by the TRI pattern in our study area and demonstrated by our within-survey TCPs, which were too small. This impact is also dependent on the spot-size effect of the camera and thus hard to quantify. Additionally, the surrounding terrain of the landform cause complex scattering mechanics that likely impact local adjacency effects in the study site. Furthermore, the internal settings of the pix4d software while mosaicking the individual images can lead to a distortion of the observed surface temperatures. Again, a quantification thereof was not performed in this study.

The validation was limited by the difference in physically measured temperature resulting from varying instrument measurement techniques. While the UAV TIR camera and radiometers measure radiometric skin temperature, the GST loggers observe contact skin temperature. The extraction of the UAV data in the footprint area of the radiometers and at the locations of the GST loggers is affected by mixed-pixel effects, primarily due to the large spatial heterogeneity of surface characteristics. However, other factors also play a role, including the GSD, the spot-size effect of the camera, the geolocation accuracy of the in situ data and the UAV mosaics, as well as the effects of adjacency and the mosaicking processing step in Pix4D. Furthermore, given that LST is highly variable over time, the GST loggers' rather coarse logging interval is not ideal. Nevertheless, the in situ dataset is a valuable means of validating the performance of the various correction schemes applied in this study.

5.5 Key learnings and recommendations

From our flight planning, laboratory experiments, field data acquisition, post-processing, sensitivity analysis and validation we can state a few key learnings and recommendations for UAV TIR surveys in complex environments (Figure 11). We provide a set of recommendations forming a basis for more considerations for future experiences made in this research field. They provide a guideline for points to remember and consider for each individual TIR UAV survey. Additionally, we like to state that many of these points are of relevance for any TIR UAV survey regardless of the site specific characteristics, while some are of particular importance when acquiring TIR UAV data in complex environments (marked with * in Figure 11).

https://doi.org/10.5194/egusphere-2026-787
Preprint. Discussion started: 18 February 2026

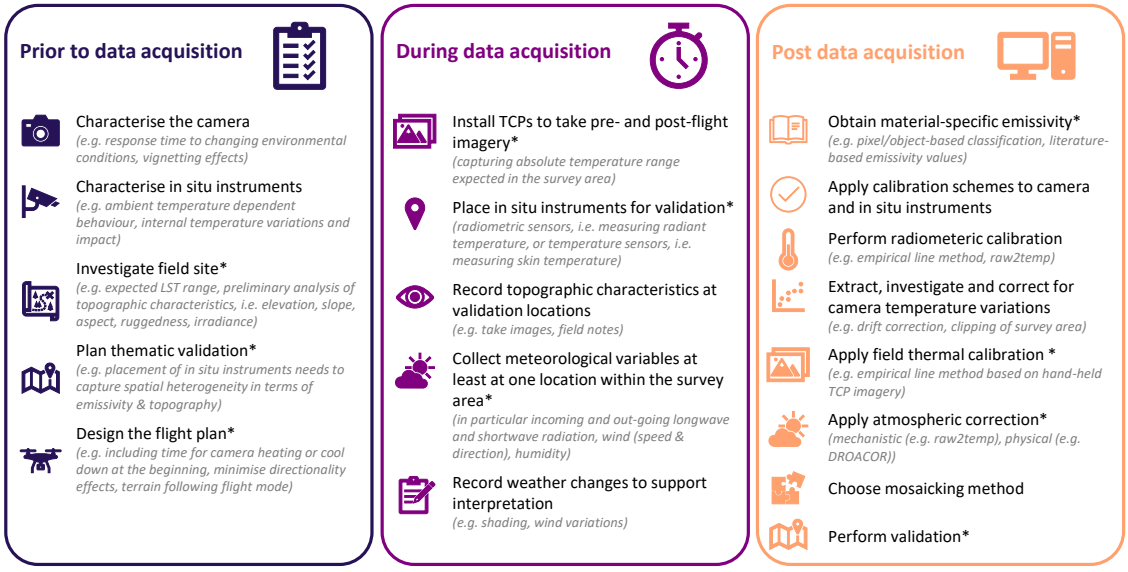

Figure 11. *Recommendations for TIR UAV surveys in complex environments. Asterisks (*) mark most important tasks to specifically consider in complex environments.*

6 Conclusions

Mountain regions constitute complex environments and are known to change rapidly. Integrative monitoring strategies are required to capture processes related to surface temperature and ultimately the surface energy budget. These strategies should encompass a range of instruments and measurements. TIR cameras mounted on UAVs offer great potential for monitoring surface temperature in complex environments. However, known challenges such as camera - pixel temperature dependency and adjacency effects have primarily been investigated in modelling studies, laboratory settings or rather homogeneous, flat environments. This study focused on complex environments that may be particularly susceptible to such disruptive factors.

Thoroughly investigating the heterogeneity within the survey area in terms of per-pixel received irradiance, micro-topography and surface materials is key to disentangle the impacting factors as best as possible. Our analysis has demonstrated the importance of field thermal calibration. Pre- and post-flight handheld imaging over TCPs that cover the expected surface temperature range in the survey area is crucial for building a robust calibration model taking field conditions (ambient meteorology and camera behaviour) into account. Proper characterisation of all instruments (in situ and UAV) is essential for interpreting the obtained data and applying the necessary post-processing schemes. Thematic validation adopted to the site specific characteristics greatly supports post-processing, ensuring accurate surface temperature retrieval. Comprehensive knowledge about pre- and post-processing of TIR instruments and data to obtain accurate surface temperature information is key to minimise error propagation down the processing chain such as debris-thickness, albedo and energy fluxes estimations, and related impact on melt/thaw dynamics, to name a few cryospheric examples.

https://doi.org/10.5194/egusphere-2026-787
Preprint. Discussion started: 18 February 2026

The results of this study shed light on the complexity of acquiring and processing UAV TIR data, specifically highlighting the challenges arising from complex environments. We hope similar systematic evaluations of TIR data are performed in other regions and environmental settings to work towards a common survey and processing protocol for TIR cameras on board UAVs.

Data availability. The PERMOS data can be obtained from the PERMOS webpage (PERMOS, 2025a, b). All UAV data used and produced through this study are available upon request.

https://doi.org/10.5194/egusphere-2026-787
Preprint. Discussion started: 18 February 2026

Appendix A

A1 Meteorological conditions

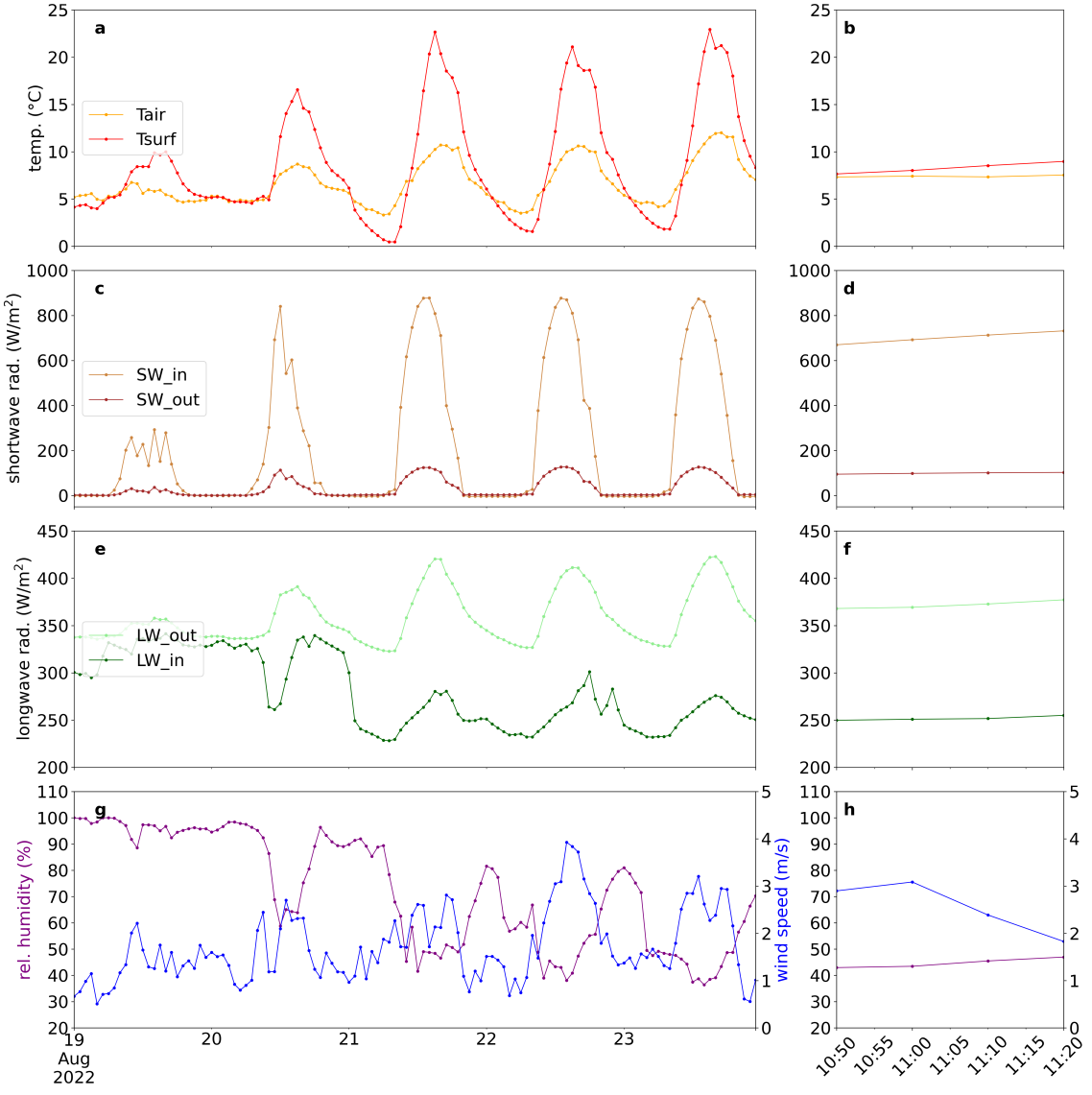

Figure A1. *Meteorological conditions at the AWS on the Murtèl rock glacier on the survey day plus four days prior (left) and during the survey (right, time shown is GPS time) in 2022 for air and surface temperature (a, b), incoming and outgoing shortwave radiation (c, d), incoming and outgoing longwave radiation (e, f), and relative humidity and wind speed (g, h).*

https://doi.org/10.5194/egusphere-2026-787
Preprint. Discussion started: 18 February 2026

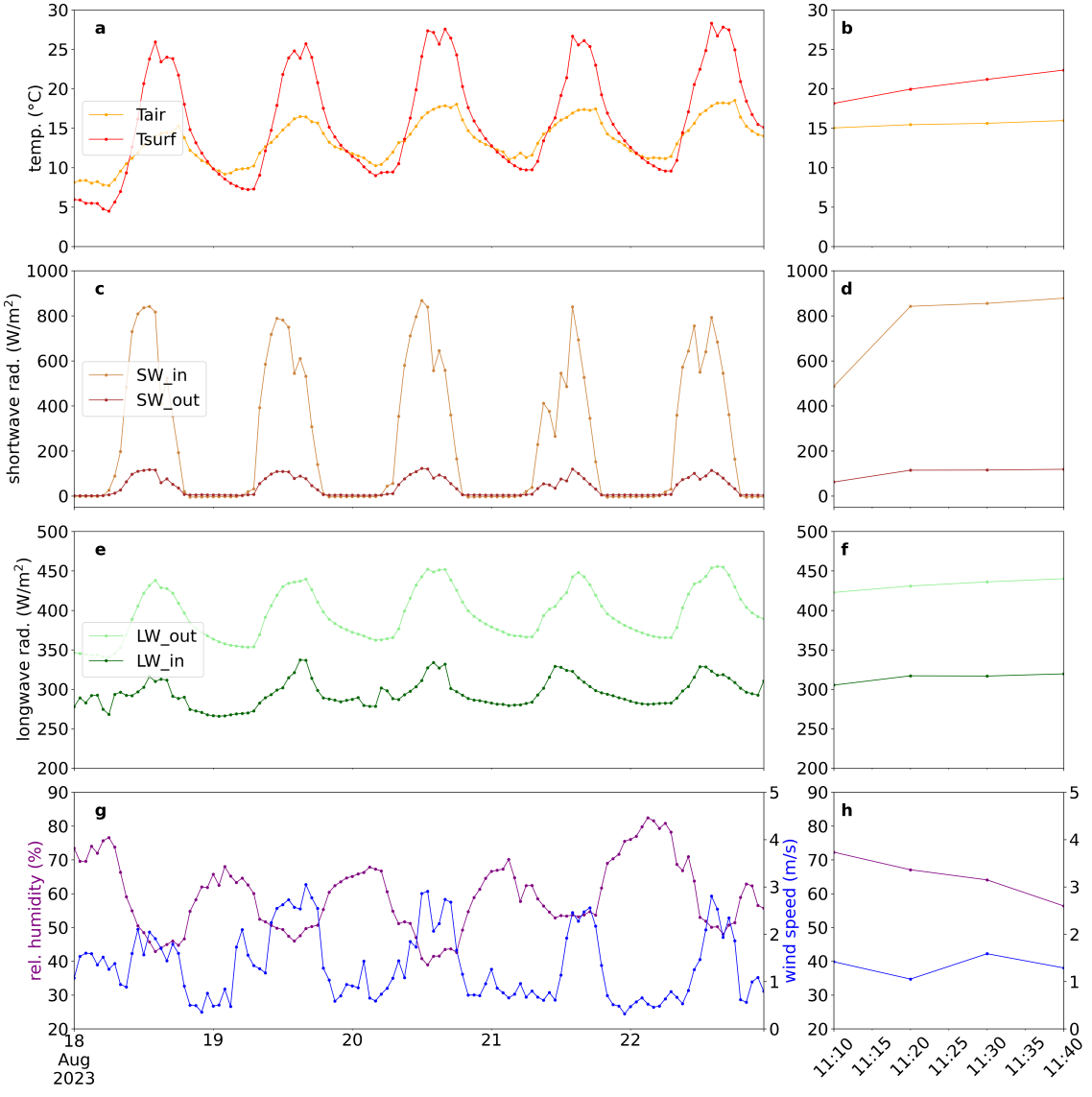

Figure A2. *Meteorological conditions at the AWS on the Murtèl rock glacier on the survey day plus four days prior (left) and during the survey (right, time shown is GPS time) in 2023 for air and surface temperature (a, b), incoming and outgoing shortwave radiation (c, d), incoming and outgoing longwave radiation (e, f), and relative humidity and wind speed (g, h).*

https://doi.org/10.5194/egusphere-2026-787
Preprint. Discussion started: 18 February 2026

A2 Sensitivity anaylsis - orthomosaic statistics

Table A1. *Statistics of each individual TIR orthomosaic and the impact of the individual correction schemes compared to the reference orthomosaic (raw).*

	TIR OM	Mean [°C]	Med [°C]	Stdv [°C]	Var [°C^2]	Min [°C]	Max [°C]	Rng [°C]	Diff [%]	Var Diff [°C^2]
2022-08-23	raw	14.31	14.49	4.82	23.21	-4.65	32.90	37.54	-	-
	drift	17.03	16.91	3.59	12.89	4.56	33.80	29.24	19.02	10.11
	lab	14.80	14.97	4.23	17.86	-1.63	31.46	33.09	3.48	0.37
2023-08-22	raw	16.41	17.11	7.05	49.67	-19.61	39.35	58.95	-	-
	drift	23.73	23.86	4.92	24.21	-3.88	46.21	50.08	44.63	26.64
	lab	16.39	17.00	6.19	38.35	-15.10	36.36	51.46	-0.11	4.42
	field	12.01	12.83	8.38	70.23	-31.40	39.00	70.40	-26.80	6.66

https://doi.org/10.5194/egusphere-2026-787
Preprint. Discussion started: 18 February 2026

A3 GST diurnal variability on the survey days

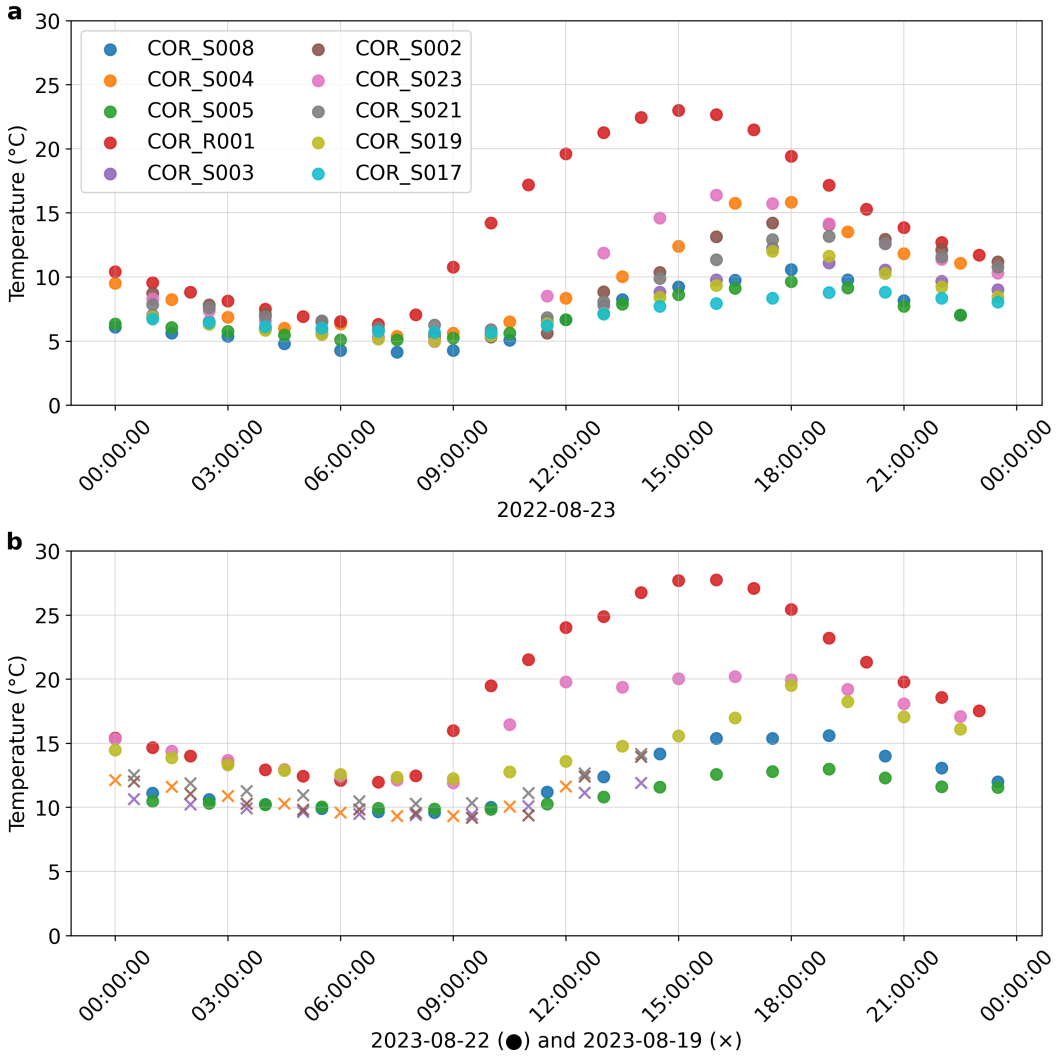

Figure A3. *(a) GST diurnal cycle on 23 August 2022 for all loggers, and (b) on 22 August 2023 for COR_S008, S005, S019, S023, R001 (dots), and on 19 August 2023 for COR_S002, S003, S004, S021 (crosses).*

https://doi.org/10.5194/egusphere-2026-787
Preprint. Discussion started: 18 February 2026

A4 Topographic impact assessment

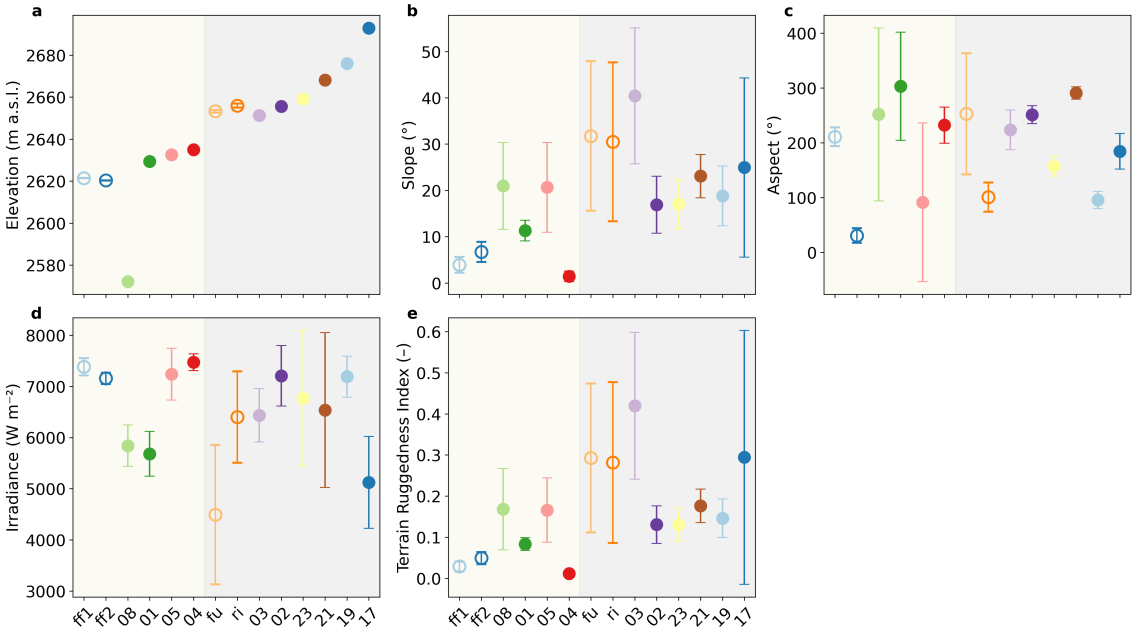

Figure A4. *Topographic characteristics elevation (a), slope (b), aspect (c), irradiance (d) and Terrain Ruggedness Index (TRII (e) at each in situ location. GST locations are depicted as dots, TIR radiometer locations as circles. Errorbars indicate the standard deviation of all values extracted within the footprint of each location. The beige shaded area comprises instruments located in the forefield or on the relict rock glacier, while the grey shaded area comprises all instruments located on the active rock glacier.*

https://doi.org/10.5194/egusphere-2026-787
Preprint. Discussion started: 18 February 2026

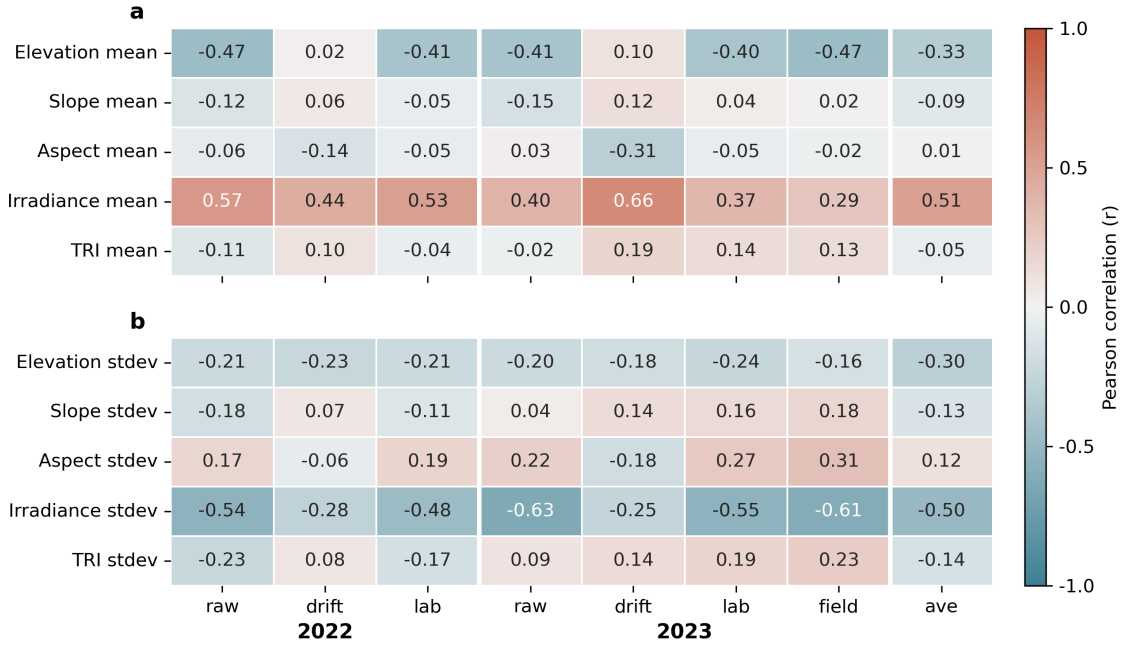

Figure A5. *Pearson correlation coefficients between in situ and UAV TIR absolute temperature differences and topographic factors. (a) Mean values of elevation, slope, aspect, irradiance, and Terrain Ruggedness Index (TRI). (b) Standard deviations of the same factors, representing local heterogeneity. Positive and negative correlations are displayed in red and blue, respectively.*

https://doi.org/10.5194/egusphere-2026-787
Preprint. Discussion started: 18 February 2026

Author contributions. **KN:** Writing – original draft, Writing – review & editing, Visualization, Validation, Methodology, Investigation, Formal analysis, Data acquisition & curation, Conceptualization. **JSA:** Writing – review & editing, Visualization, Validation, Methodology, Investigation, Formal analysis, Data acquisition & curation, Conceptualization. **GB:** Writing – review & editing, Data acquisition. **IGR:** Writing – review & editing, Validation, Data acquisition & curation. **JG:** Writing – review & editing, Validation, Methodology, Data acquisition & curation. **NR:** Writing – review & editing, Visualization, Validation, Methodology, Investigation, Formal analysis, Data acquisition & curation.

Competing interests. The authors declare that they have no conflict of interest.

Acknowledgements. KN, JSA and NR are supported by the ESA PRODEX Trishna T-SEC project (PEA C4000133711). GB is supported by the SNSF Ambizione project grant no. 216385.

https://doi.org/10.5194/egusphere-2026-787
Preprint. Discussion started: 18 February 2026

References

Adams, J. S., Damm, A., Werfeli, M., Gröbner, J., and Naegeli, K.: Across-scale thermal infrared anisotropy in forests: Insights from a multi-angular laboratory-based approach, Remote Sensing of Environment, 326, 114 766, https://doi.org/10.1016/J.RSE.2025.114766, 2025.

Aragon, B., Johansen, K., Parkes, S., Malbeteau, Y., Al-mashharawi, S., Al-amoudi, T., Andrade, C. F., Turner, D., Lucieer, A., and McCabe, M. F.: A Calibration Procedure for Field and UAV-Based Uncooled Thermal Infrared Instruments, Sensors 2020, Vol. 20, Page 3316, 20, 3316, https://doi.org/10.3390/S20113316, 2020.

Arioli, S., Picard, G., Arnaud, L., Gascoin, S., Alonso-González, E., Poizat, M., and Irvine, M.: Time series of alpine snow surface radiative-temperature maps from high-precision thermal-infrared imaging, Earth System Science Data, 16, 3913–3934, https://doi.org/10.5194/ESSD-16-3913-2024, 2024.

Aubrecht, D. M., Helliker, B. R., Goulden, M. L., Roberts, D. A., Still, C. J., and Richardson, A. D.: Continuous, long-term, high-frequency thermal imaging of vegetation: Uncertainties and recommended best practices, Agricultural and Forest Meteorology, 228-229, 315–326, https://doi.org/10.1016/j.agrformet.2016.07.017, 2016.

Aubry-Wake, C., Lamontagne-Hallé, P., Baraër, M., McKenzie, J. M., and Pomeroy, J. W.: Using ground-based thermal imagery to estimate debris thickness over glacial ice: fieldwork considerations to improve the effectiveness, Journal of Glaciology, pp. 1–17, https://doi.org/10.1017/jog.2022.67, 2022.

Bhardwaj, A., Sam, L., Akanksha, Martín-Torres, F. J., and Kumar, R.: UAVs as remote sensing platform in glaciology: Present applications and future prospects, Remote Sensing of Environment, 175, 196–204, https://doi.org/10.1016/J.RSE.2015.12.029, 2016.

Bisset, R. R., Nienow, P. W., Goldberg, D. N., Wigmore, O., Loayza-Muro, R. A., Wadham, J. L., Macdonald, M. L., and Bingham, R. G.: Using thermal UAV imagery to model distributed debris thicknesses and sub-debris melt rates on debris-covered glaciers, Journal of Glaciology, 69, 981–996, https://doi.org/10.1017/JOG.2022.116, 2023.

Brenning, A., Peña, M. A., Long, S., and Soliman, A.: Thermal remote sensing of ice-debris landforms using ASTER: An example from the Chilean Andes, The Cryosphere, 6, 367–382, https://doi.org/10.5194/TC-6-367-2012, 2012.

Casas-Mulet, R., Pander, J., Ryu, D., Stewardson, M. J., and Geist, J.: Unmanned Aerial Vehicle (UAV)-Based Thermal Infra-Red (TIR) and Optical Imagery Reveals Multi-Spatial Scale Controls of Cold-Water Areas Over a Groundwater-Dominated Riverscape, Frontiers in Environmental Science, 8, 534 986, https://doi.org/10.3389/FENVS.2020.00064/BIBTEX, 2020.

Cawse-Nicholson, K., Townsend, P. A., Schimel, D., Assiri, A. M., Blake, P. L., Buongiorno, M. F., Campbell, P., Carmon, N., Casey, K. A., Correa-Pabón, R. E., Dahlin, K. M., Dashti, H., Dennison, P. E., Dierssen, H., Erickson, A., Fisher, J. B., Frouin, R., Gatebe, C. K., Gholizadeh, H., Gierach, M., Glenn, N. F., Goodman, J. A., Griffith, D. M., Guild, L., Hakkenberg, C. R., Hochberg, E. J., Holmes, T. R., Hu, C., Hulley, G., Huemmrich, K. F., Kudela, R. M., Kokaly, R. F., Lee, C. M., Martin, R., Miller, C. E., Moses, W. J., Muller-Karger, F. E., Ortiz, J. D., Otis, D. B., Pahlevan, N., Painter, T. H., Pavlick, R., Poulter, B., Qi, Y., Realmuto, V. J., Roberts, D., Schaepman, M. E., Schneider, F. D., Schwandner, F. M., Serbin, S. P., Shiklomanov, A. N., Stavros, E. N., Thompson, D. R., Torres-Perez, J. L., Turpie, K. R., Tzortziou, M., Ustin, S., Yu, Q., Yusup, Y., and Zhang, Q.: NASA's surface biology and geology designated observable: A perspective on surface imaging algorithms, Remote Sensing of Environment, 257, 112 349, https://doi.org/10.1016/J.RSE.2021.112349, 2021.

Colombo, R., Pennati, G., Pozzi, G., Garzonio, R., Di Mauro, B., Giardino, C., Cogliati, S., Rossini, M., Maltese, A., Pogliotti, P., and Cremonese, E.: Mapping snow density through thermal inertia observations, Remote Sensing of Environment, 284, 113 323, https://doi.org/10.1016/J.RSE.2022.113323, 2023.

https://doi.org/10.5194/egusphere-2026-787
Preprint. Discussion started: 18 February 2026

Colomina, I. and Molina, P.: Unmanned aerial systems for photogrammetry and remote sensing: A review, ISPRS Journal of Photogrammetry and Remote Sensing, 92, 79–97, https://doi.org/10.1016/J.ISPRSJPRS.2014.02.013, 2014.

Crago, R. D. and Qualls, R. J.: Use of land surface temperature to estimate surface energy fluxes: Contributions of Wilfried Brutsaert and collaborators, Water Resources Research, 50, 3396–3408, https://doi.org/10.1002/2013WR015223, 2014.

Dugdale, S. J., Kelleher, C. A., Malcolm, I. A., Caldwell, S., and Hannah, D. M.: Assessing the potential of drone-based thermal infrared imagery for quantifying river temperature heterogeneity, Hydrological Processes, 33, 1152–1163, https://doi.org/10.1002/HYP.13395, 2019.

Elfarkh, J., Johansen, K., Angulo, V., Camargo, O. L., and McCabe, M. F.: Quantifying Within-Flight Variation in Land Surface Temperature from a UAV-Based Thermal Infrared Camera, Drones 2023, Vol. 7, Page 617, 7, 617, https://doi.org/10.3390/DRONES7100617, 2023.

Gök, D. T., Scherler, D., and Anderson, L. S.: High-resolution debris-cover mapping using UAV-derived thermal imagery: Limits and opportunities, The Cryosphere, 17, 1165–1184, https://doi.org/10.5194/TC-17-1165-2023, 2023.

Gröbner, J.: Operation and investigation of a tilted bottom cavity for pyrgeometer characterizations, Applied Optics, 47, 4441–4447, https://doi.org/10.1364/AO.47.004441, 2008.

Groos, A. R., Aeschbacher, R., Fischer, M., Kohler, N., Mayer, C., and Senn-Rist, A.: Accuracy of UAV Photogrammetry in Glacial and Periglacial Alpine Terrain: A Comparison With Airborne and Terrestrial Datasets, Frontiers in Remote Sensing, 3, 871 994, https://doi.org/10.3389/FRSEN.2022.871994/BIBTEX, 2022.

Gärtner-Roer, I. and Hoelzle, M.: Rockglaciers of the Engadine, World Geomorphological Landscapes, pp. 235–248, https://doi.org/10.1007/978-3-030-43203-4_16/FIGURES/9, 2021.

Hoelzle, M., Hauck, C., Mathys, T., Noetzli, J., Pellet, C., and Scherler, M.: Long-term energy balance measurements at three different mountain permafrost sites in the Swiss Alps, Earth System Science Data, 14, 1531–1547, https://doi.org/10.5194/ESSD-14-1531-2022, 2022.

Hook, S. J., Johnson, W. R., and Abrams, M. J.: NASA's Hyperspectral Thermal Emission Spectrometer (HyTES), Remote Sensing and Digital Image Processing, 17, 93–115, https://doi.org/10.1007/978-94-007-6639-6_5, 2013.

Huo, D., Bishop, M. P., and Bush, A. B.: Understanding Complex Debris-Covered Glaciers: Concepts, Issues, and Research Directions, Frontiers in Earth Science, 9, 652 279, https://doi.org/10.3389/FEART.2021.652279/XML, 2021.

Kelly, J., Kljun, N., Olsson, P. O., Mihai, L., Liljeblad, B., Weslien, P., Klemedtsson, L., and Eklundh, L.: Challenges and best practices for deriving temperature data from an uncalibrated UAV thermal infrared camera, Remote Sensing, 11, https://doi.org/10.3390/rs11050567, 2019.

Koetz, B., Bastiaanssen, W., Berger, M., Defourney, P., Bello, U. D., Drusch, M., Drinkwater, M., Duca, R., Fernandez, V., Ghent, D., Guzinski, R., Hoogeveen, J., Hook, S., Lagouarde, J. P., Lemoine, G., Manolis, I., Martimort, P., Masek, J., Massart, M., Notarnicola, C., Sobrino, J., and Udelhoven, T.: High spatio-temporal resolution land surface temperature mission - A copernicus candidate mission in support of agricultural monitoring, International Geoscience and Remote Sensing Symposium (IGARSS), 2018-July, 8160–8162, https://doi.org/10.1109/IGARSS.2018.8517433, 2018.

Kraaijenbrink, P. D., Shea, J. M., Pellicciotti, F., Jong, S. M., and Immerzeel, W. W.: Object-based analysis of unmanned aerial vehicle imagery to map and characterise surface features on a debris-covered glacier, Remote Sensing of Environment, 186, 581–595, https://doi.org/10.1016/J.RSE.2016.09.013, 2016.

Kraaijenbrink, P. D., Shea, J. M., Litt, M., Steiner, J. F., Treichler, D., Koch, I., and Immerzeel, W. W.: Mapping surface temperatures on a debris-covered glacier with an unmanned aerial vehicle, Frontiers in Earth Science, 6, https://doi.org/10.3389/feart.2018.00064, 2018.

https://doi.org/10.5194/egusphere-2026-787
Preprint. Discussion started: 18 February 2026

Lillesand, T., Kiefer, R. W., and Chipman, J. W.: Remote Sensing and Image Interpretation, John Wiley & Sons Ltd, seventh ed edn., ISBN 978-1-118-34328-9, 2015.

Lin, D., Maas, H. G., Westfeld, P., Budzier, H., and Gerlach, G.: An advanced radiometric calibration approach for uncooled thermal cameras, The Photogrammetric Record, 33, 30–48, https://doi.org/10.1111/PHOR.12216, 2018.

Liu, Y., Hiyama, T., and Yamaguchi, Y.: Scaling of land surface temperature using satellite data: A case examination on ASTER and MODIS products over a heterogeneous terrain area, Remote Sensing of Environment, 105, 115–128, https://doi.org/10.1016/J.RSE.2006.06.012, 2006.

Maes, W. H., Huete, A. R., and Steppe, K.: Optimizing the processing of UAV-based thermal imagery, Remote Sensing, 9, https://doi.org/10.3390/rs9050476, 2017.

Malbéteau, Y., Johansen, K., Aragon, B., Al-Mashhawari, S. K., and McCabe, M. F.: Overcoming the Challenges of Thermal Infrared Orthomosaics Using a Swath-Based Approach to Correct for Dynamic Temperature and Wind Effects, Remote Sensing, 13, 3255, https://doi.org/10.3390/RS13163255, 2021.

Mesas-Carrascosa, F. J., Pérez-Porras, F., de Larriva, J. E. M., Frau, C. M., Agüera-Vega, F., Carvajal-Ramírez, F., Martínez-Carricondo, P., and García-Ferrer, A.: Drift Correction of Lightweight Microbolometer Thermal Sensors On-Board Unmanned Aerial Vehicles, Remote Sensing 2018, Vol. 10, Page 615, 10, 615, https://doi.org/10.3390/RS10040615, 2018.

Messmer, J. and Groos, A. R.: A low-cost and open-source approach for supraglacial debris thickness mapping using UAV-based infrared thermography, The Cryosphere, https://doi.org/10.5194/tc-18-719-2024, 2024.

Mineo, S. and Pappalardo, G.: Rock Emissivity Measurement for Infrared Thermography Engineering Geological Applications, Applied Sciences 2021, Vol. 11, Page 3773, 11, 3773, https://doi.org/10.3390/APP11093773, 2021.

O'sullivan, A. M. and Kurylyk, B. L.: Limiting External Absorptivity of UAV-Based Uncooled Thermal Infrared Sensors Increases Water Temperature Measurement Accuracy, Remote Sensing, 14, https://doi.org/https://doi.org/10.3390/rs14246356, 2022.

Pepin, N., Apple, M., Knowles, J., Terzago, S., Arnone, E., Hänchen, L., Napoli, A., Potter, E., Steiner, J., Williamson, S. N., Ahrens, B., Dhar, T., Dimri, A. P., Palazzi, E., Rameshan, A., Salzmann, N., Shahgedanova, M., de Deus Vidal, J., and Zardi, D.: Elevation-dependent climate change in mountain environments, Nature Reviews Earth & Environment 2025 6:12, 6, 772–788, https://doi.org/10.1038/s43017-025-00740-4, 2025.

Pepin, N. C., Arnone, E., Gobiet, A., Haslinger, K., Kotlarski, S., Notarnicola, C., Palazzi, E., Seibert, P., Serafin, S., Schöner, W., Terzago, S., Thornton, J. M., Vuille, M., and Adler, C.: Climate Changes and Their Elevational Patterns in the Mountains of the World, Reviews of Geophysics, 60, e2020RG000 730, https://doi.org/10.1029/2020RG000730, 2022.

PERMOS: Swiss Permafrost Monitoring Network Database (PERMOS Database), https://doi.org/10.13093/permos-2025-01, 2025a.

PERMOS: Swiss Permafrost Bulletin 2024, 6 edn., https://doi.org/10.13093/permos-bull-2025, 2025b.

Pignatti, S., Lapenna, V., Palombo, A., Pascucci, S., Pergola, N., and Cuomo, V.: An advanced tool of the CNR IMAA EO facilities: Overview of the TASI-600 hyperspectral thermal spectrometer, Workshop on Hyperspectral Image and Signal Processing, Evolution in Remote Sensing, https://doi.org/10.1109/WHISPERS.2011.6080890, 2011.

Rietze, N., Assmann, J. J., Plekhanova, E., Naegeli, K., Damm, A., Maximov, T. C., Karsanaev, S. V., Hensgens, G., and Schaepman-Strub, G.: Summer drought weakens land surface cooling of tundra vegetation, Environmental Research Letters, 19, 044 043, https://doi.org/10.1088/1748-9326/AD345E, 2024.

Riley, S. J., DeGloria, S. D., and Elliot, R.: A terrain ruggedness index that quantifies topographic heterogeneity, Intermountain Journal of Science, 5, 23–27, 1999.

https://doi.org/10.5194/egusphere-2026-787
Preprint. Discussion started: 18 February 2026

Roujean, J. L., Bhattacharya, B., Gamet, P., Pandya, M. R., Boulet, G., Olioso, A., Singh, S. K., Shukla, M. V., Mishra, M., Babu, S., Raju, P. V., Murthy, C. S., Briottet, X., Rodler, A., Autret, E., Dadou, I., Adlakha, D., Sarkar, M., Picard, G., Kouraev, A., Ferrari, C., Irvine, M., Delogu, E., Vidal, T., Hagolle, O., Maisongrande, P., Sekhar, M., and Mallick, K.: TRISHNA: An Indo-French Space Mission to Study the Thermography of the Earth at Fine Spatio-Temporal Resolution, 2021 IEEE India Geoscience and Remote Sensing Symposium, InGARSS 2021 - Proceedings, pp. 49–52, https://doi.org/10.1109/INGARSS51564.2021.9791925, 2021.

Rubio, E., Caselles, V., and Badenas, C.: Emissivity measurements of several soils and vegetation types in the 8–14, μm Wave band: Analysis of two field methods, Remote Sensing of Environment, 59, 490–521, https://doi.org/10.1016/S0034-4257(96)00123-X, 1997.

Saibene, G., Gärtner-Roer, I., Beutel, J., and Vieli, A.: Multi-annual and seasonal patterns of Murtèl rock glacier borehole deformation, environmental controls and implications for kinematic monitoring, The Cryosphere Discussions, https://doi.org/10.5194/EGUSPHERE-2025-3029, 2025.

Tattersall, G.: gtatters/Thermimage: Thermimage v4.1.3, https://doi.org/10.5281/zenodo.5525416, 2021.

Wan, Q., Smigaj, M., Brede, B., and Kooistra, L.: Optimizing UAV-based uncooled thermal cameras in field conditions for precision agriculture, International Journal of Applied Earth Observation and Geoinformation, 134, 104 184, https://doi.org/10.1016/J.JAG.2024.104184, 2024.

Wang, Z., Zhou, J., Ma, J., Wang, Y., Liu, S., Ding, L., Tang, W., Pakezhamu, N., and Meng, L.: Removing temperature drift and temporal variation in thermal infrared images of a UAV uncooled thermal infrared imager, ISPRS Journal of Photogrammetry and Remote Sensing, 203, 392–411, https://doi.org/10.1016/J.ISPRSJPRS.2023.08.011, 2023.

Wigmore, O. and Molotch, N. P.: Weekly high-resolution multi-spectral and thermal uncrewed-aerial-system mapping of an alpine catchment during summer snowmelt, Niwot Ridge, Colorado, Earth System Science Data, 15, 1733–1747, https://doi.org/10.5194/ESSD-15-1733-2023, 2023.